Perfect Absorption in Mirror-Symmetric Acoustic Metascreens

V. Romero-García,[1,*] N. Jiménez,[2] J.-P. Groby,[1] A. Merkel,[3] V. Tournat,[1] G. Theocharis,[1] O. Richoux,[1] and V. Pagneux[1]

[1] *Laboratoire d'Acoustique de l'Université du Mans (LAUM), UMR 6613, Institut d'Acoustique–Graduate School (IA-GS), CNRS, Le Mans Université, Avenue Olivier Messiaen, 72085 Le Mans, France*

[2] *Instituto de Instrumentación para Imagen Molecular, Consejo Superior de Investigaciones Científicas, Universitat Politècnica de València, Camino de vera s/n, València 46022, Spain*

[3] *Institut Jean Lamour, University of Lorraine, 2 allée André Guinier, 54011 Nancy, France*

(Received 21 July 2020; accepted 1 October 2020; published 20 November 2020)

Mirror-symmetric acoustic metascreens producing perfect absorption independently of the incidence side are theoretically and experimentally reported in this work. The mirror-symmetric resonant building blocks of the metascreen support symmetric and antisymmetric resonances that can be tuned to be at the same frequency (degenerate resonances). The geometry of the building blocks is optimized to critically couple both the symmetric and the antisymmetric resonances at the same frequency, allowing perfect absorption of sound from both sides of the metascreen. A hybrid analytical model based on the transfer-matrix method and the modal decomposition of the exterior acoustic field is developed to analyze the scattering properties of the metascreen. The resulting geometry is three-dimensionally printed and experimentally tested in an impedance tube. The experimental results agree well with the theoretical predictions, proving the efficiency of these metascreens for the perfect absorption of sound in ventilation problems.

DOI: 10.1103/PhysRevApplied.14.054055

I. INTRODUCTION

Perfect absorption with subwavelength materials is a scientific and technological challenge that has attracted increasing interest over recent years in several branches of wave physics [1–8]. To meet such a challenge, a twofold problem must be solved: the ratio of the wavelength of the absorbed wave to the size of the systems must reach values much larger than one and, at the same time, the impedance of the system must match that of the surrounding medium. Acoustic metamaterials made of open lossy resonators have been proven to be very good candidates to meet these two conditions [4,9–14]. They offer the possibility of tuning their inherent losses in a controlled manner and their subwavelength character has already been exploited to design perfect absorbers in both the reflection problem [12,15] and the transmission problem [13,14,16].

Previously, perfect absorption has been successfully analyzed using the properties of the scattering matrix of the system [17]. In a general manner, perfect absorption can be obtained at the frequencies for which the eigenvalues of the scattering matrix are zero and when the system is excited with the corresponding eigenvectors [17]. From the physical point of view, zero eigenvalues of the scattering matrix appear when the critical-coupling condition is fulfilled, i.e., when the energy leakage of the system is perfectly balanced by its inherent losses [10]. In a reflection problem (a one-port problem), the scattering matrix reduces to the reflection coefficient. The critical-coupling conditions have been exploited to design deep subwavelength absorbers making use of Helmholtz resonators (HRs) [9–11,18,19], membranes [4,9,15,20,21], coiled-up channels [22–24], bubble screens in water [7,25], structured surfaces [26], or slow-sound metamaterials [12,27,28]. In transmission problems (in a two-port system with one-sided excitation), the analysis becomes more complicated and depending on the symmetry of the acoustic metamaterial, one can deal with two types of problems. If the metamaterial is not mirror symmetric, the scattering on each side of the structure is different, giving rise to different absorption coefficients on the two sides [29,30]. At a specific frequency, the critical-coupling condition can be fulfilled on one of the sides of the acoustic metamaterial and, as a consequence, single-sided unidirectional perfect absorption can be obtained [17]. This unidirectional perfect absorption has been obtained using HRs to design slow-sound-type metasurfaces [13]. If the metamaterial is mirror symmetric, perfect absorption can be obtained on the two sides of the system but the problem becomes more complicated as a symmetric and an antisymmetric resonance occurring at the same frequency (degenerate resonances) must be activated [3,16]. It is worth

*vicente.romero@univ-lemans.fr

 © 2020 American Physical Society

noting here that if two resonances in mirror-symmetric systems have the same symmetry, the absorption cannot be perfect. However, quasiperfect absorption can be obtained using an accumulation point to bring symmetric and antisymmetric resonances as close as possible to each other [31]. Thus, the main challenge here is the design of the resonant building blocks presenting degenerate resonances.

In this work, we design a metascreen made of mirror-symmetric resonant building blocks possessing degenerate resonances to produce perfect acoustic absorption on the two sides of the metascreen, by the simultaneous critical coupling of both symmetric and antisymmetric resonances. The metascreen consists of a periodic array of slits loaded by different HRs. The resonant mirror-symmetric building block of this metascreen presents both symmetric and antisymmetric resonances, allowing for the critical coupling of the transmission problem. The system is analytically studied by a hybrid model combining the transfer-matrix and modal-decomposition methods. The transfer-matrix model is used to describe the propagation within each slit, while modal decomposition is used to obtain the propagation in the exterior domain considering the Bloch waves accounting for the possible evanescent coupling between the slits. The two domains are coupled through the continuity conditions between the exterior medium and each slit. A full-wave numerical simulation is used to validate the analytical model. The absorption of the metascreen is optimized for the transmission problem (ventilation), allowing for perfect absorption in the system from both sides. Finally, the resonant building block is three-dimensionally (3D) printed and experimentally tested in a square-cross-section impedance tube, mimicking a metascreen with infinite lateral dimensions. The experimental results agree with the analytical and numerical predictions, obtained using COMSOL MULTIPHYSICS, showing the possibility of designing perfect absorbers for the transmission problem.

II. RECIPROCAL AND SYMMETRIC UNIDIMENSIONAL SCATTERING: SYMMETRIC AND ANTISYMMETRIC PROBLEMS

In this section, we show that the scattering problem by a mirror-symmetric scatterer can be decomposed into two reflection subproblems [17,32]: (i) the symmetric reflection problem, which is produced when the Neumann boundary condition is imposed at the mirror-symmetry plane of the mirror-symmetric resonator; and (ii) the antisymmetric reflection problem, which is produced when the Dirichlet boundary condition is imposed at the mirror-symmetry plane of the mirror-symmetric resonator.

A reciprocal and symmetric unidimensional (1D) scattering problem is characterized by a symmetric scattering matrix,

$$S(\omega) = \begin{pmatrix} T & R \\ R & T \end{pmatrix}, \tag{1}$$

where R and T are the complex frequency-dependent reflection and transmission coefficients of the system, respectively. The absorption coefficient can thus be defined as $\alpha = 1 - |R|^2 - |T|^2$. The eigenvalues of the scattering matrix are given by $\lambda_\pm = T \pm R$, while the eigenvectors are $\vec{v}_\pm = (1, \pm 1)$. Figure 1(a) represents the scattering problem when a symmetric system {symmetry with respect to the median plane [white dashed line in Fig. 1(a)]} is excited by a plane wave from the left with the harmonic time convention $e^{-i\omega t}$. First, we consider that a Neumann boundary condition $\partial p/\partial x = 0$ is imposed at the symmetry plane of the system, p representing the pressure wave that is the solution of the Helmholtz equation [see Fig. 1(b)]. The Neumann boundary condition imposes a perfect mirror symmetry, creating a virtual image of the full problem on the right-hand side. Therefore, the reflection coefficient of this particular subproblem, R_s, can be calculated from the reflection and transmission coefficients of the original problem, $R_s = T + R$. The subindex s means symmetric since the Neumann boundary condition selects only modes that are symmetric with respect to the symmetry plane where the condition is imposed. Second, we consider that a Dirichlet boundary condition, $p = 0$, is imposed at the mirror-symmetry plane of the system. This plane acts as a mirror, creating a virtual image on the right-hand side with

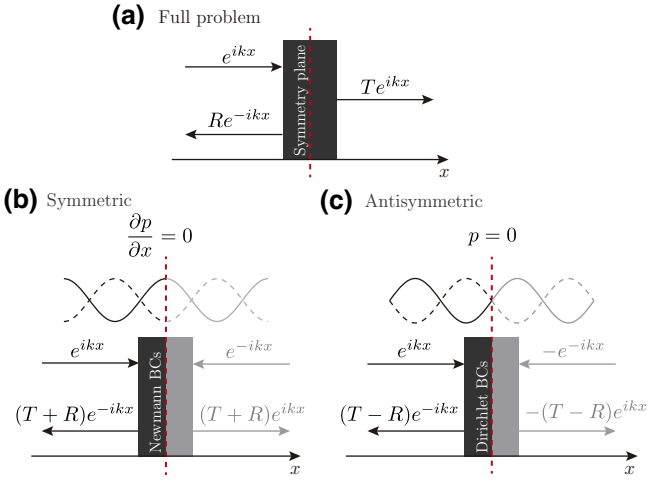

FIG. 1. (a) The 1D transmission problem of a plane wave by a mirror-symmetric resonant scatterer. (b),(c) The reflection problem produced when a Neumann and a Dirichlet boundary conditions are, respectively, considered in the symmetry plane of the symmetric resonant scatterer [red dashed lines in (b) and (c)]. The continuous line represents the incident pressure wave and the dashed line represents the reflected wave due to the boundary condition. The image generated by the presence of the boundary condition is represented in gray.

a π phase shift of the full problem. The reflection coefficient of this particular subproblem, R_a, can be calculated from the reflection and transmission coefficients of the original one, $R_a = T - R$. The subindex a means antisymmetric since the Dirichlet boundary condition imposes only antisymmetric modes with respect to the symmetry plane. Note that the two eigenvalues of the scattering matrix of the original problem, λ_+ and λ_-, correspond to the reflection coefficients of the reflection subproblems with Neumann and Dirichlet conditions, respectively. In other words, the original transmission problem can be decomposed into the symmetric reflection problem, $\lambda_+ = R_s$, and the antisymmetric reflection problem, $\lambda_- = R_a$. Thus, the original scattering coefficients read as follows:

$$R = \frac{R_s - R_a}{2}, \quad T = \frac{R_s + R_a}{2}, \quad \alpha = \frac{\alpha_s + \alpha_a}{2}, \qquad (2)$$

where $\alpha_s = 1 - |R_s|^2$ and $\alpha_a = 1 - |R_a|^2$ are the absorption coefficients of the reflection subproblems with Neumann and Dirichlet boundary conditions, respectively.

III. MIRROR-SYMMETRIC RESONATORS WITH DEGENERATE RESONANCES FOR VENTILATION PROBLEMS

Perfect absorption in 1D reciprocal problems with one-sided excitation appears when the two eigenvalues of the scattering matrix simultaneously vanish at the same frequency [13,17]. In other words, perfect absorption in mirror-symmetric 1D reciprocal problems is achieved when the symmetric and the antisymmetric reflection problems are critically coupled simultaneously at the same frequency. In this case, $\alpha_s = \alpha_a = 1$ and thus $\alpha = 1$. This means that we need degenerate resonances to perfectly absorb waves, i.e., resonators with both symmetric and antisymmetric resonances at the same frequency. Note that if only symmetric or antisymmetric resonances are excited, only half of the problem can be critically coupled; thus the maximal absorption that can be reached is $\alpha = 0.5$.

In this section, we use systems made of slits loaded by different HRs embedded in a waveguide of different cross section. First, we analyze the propagation in a slit loaded with a single resonator, as shown in the inset of Fig. 2(a). We choose a resonator with a resonance frequency at $f_{\mathrm{HR}} = 735$ Hz. The scattering coefficients of the system are shown in Fig. 2(a). The first mode of the slit, i.e., a Fabry-Pérot resonance, is shifted at a frequency lower than f_{HR} because of the strong dispersion introduced by the loading resonator. This mode translates in the form of a transmission peak. Figure 2(c) shows the absolute value of the total pressure field at this particular frequency, showing the first resonance mode of the slit. It is worth noting here that this resonance mode is symmetric with respect to the symmetry plane of the system. Second, we analyze the propagation through a slit loaded by two HRs, as shown in the inset of Fig. 2(b). In this case, the scattering coefficients are plotted in Fig. 2(b), showing two transmission peaks corresponding to the first two Fabry-Pérot resonances of the slit. The two first resonances of the slit are clearly visible in Figs. 2(d) and 2(e), which depict the absolute value of the total pressure field at these particular frequencies. The first mode is symmetric while the second mode is antisymmetric with respect to the symmetry plane of the system [shown by the dashed line in Figs. 2(c)–2(e)].

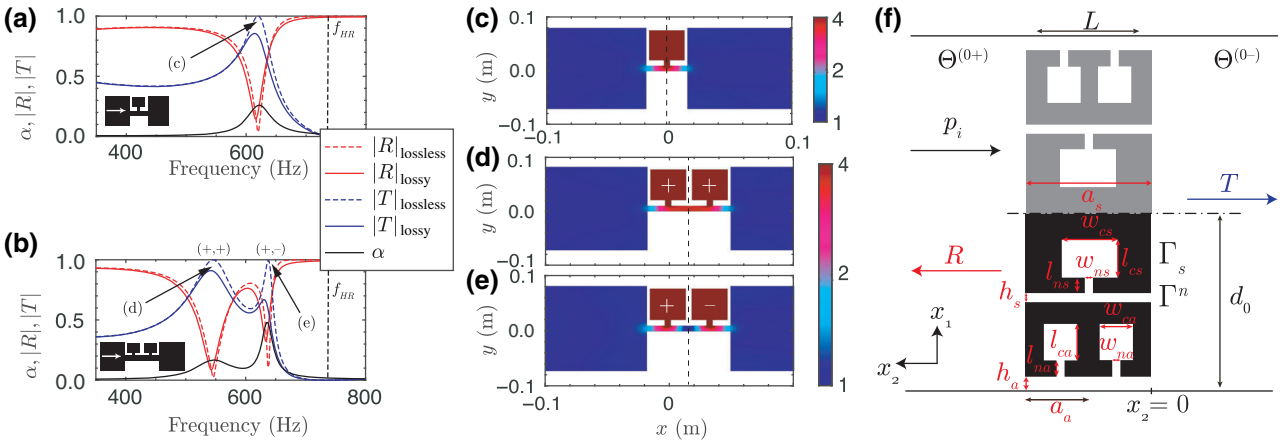

FIG. 2. (a),(b) The lossless (dashed lines) and lossy (continuous lines) scattering coefficients for the case of a slit loaded by one and two identical resonators, respectively. (c) The absolute value of the total pressure field for the frequency of the first resonance of the slit loaded with one resonator. The vertical dashed line shows the symmetry plane of the metascreen. (d),(e) The absolute value of the total pressure field for the two first resonances of the slit loaded with two identical resonators. The vertical dashed line shows the symmetry plane of the metascreen. (f) The scheme of the mirror-symmetric building block used in this work, with the definitions of the geometric parameters.

From the previous discussion, we can conclude that resonators with symmetric and antisymmetric resonances can be designed with the combination of the two discussed systems, a periodic arrangement of two slits loaded, respectively, with one and two HRs. As a consequence, the metascreen design that we propose in this work, shown in Fig. 2(f), is a combination of slits loaded by one and two resonators. The slit loaded by a single resonator only supports symmetric modes and will thus be named the "symmetric slit." The slit loaded by two resonators supports both symmetric and antisymmetric modes. It will mainly be used to tune the antisymmetric resonance and will thus be named the "antisymmetric slit." The geometric parameters of the metascreen are defined in Fig. 2(f). The subindex s (a) represents the parameters for the symmetric (antisymmetric) slit. The HRs are made by combining two different elements that play the role of the neck and the cavity. The problem consists in critically coupling the symmetric and the antisymmetric slits at the same frequency by optimizing the geometry, which controls the energy leakage and the inherent losses (viscothermal losses).

At this stage, we have to discuss the unit-cell geometry shown in Fig. 2(f). For the experiments, we only have to consider half of it [the black areas in Fig. 2(f)], as we are using a square impedance tube of side d_0. In fact, the walls of the impedance tube act as mirrors generating the virtual images [the gray areas in Fig. 2(f)] with respect to the position of the rigid wall in the tube, i.e., the dot-dashed line in Fig. 2(f).

IV. MODELING

The theoretical approach considered in this work is a hybrid model combining the modal-decomposition and transfer-matrix methods. The modal decomposition of the acoustic field is used at the exterior domains in order to account for the Bloch modes excited at the interfaces of the metascreen possibly allowing evanescent coupling between the different building blocks. The wave propagation in each slit is modeled by the transfer-matrix method (TMM), as widely done previously [12,13].

The acoustic field in the exterior domains [Θ^{0+} and Θ^{0-} as defined in Fig. 2(f)] when the system is excited by a plane wave $\vec{k}^0 = (k_1^i, k_2^i)$ can be written as

$$p^{(0+)} = \sum_q \left[e^{-\imath k_{2q}^0 (x_2 - L)} \delta_q + R_q e^{\imath k_{2q}^0 (x_2 - L)} \right] e^{\imath k_{1q}^0 x_1} \quad \text{in } \Theta^{0+}, \tag{3}$$

$$p^{(0-)} = \sum_q T_q e^{\imath k_{1q}^0 x_1 - \imath k_{2q}^0 x_2} \quad \text{in } \Theta^{0-}, \tag{4}$$

where the subindex q indicates the order of the Bloch wave, with $k_{1q}^0 = 2q\pi / 2d_0 + k_1^i$ and $k_{2q}^0 = \sqrt{(|\vec{k}^0|)^2 - (k_{1q}^0)^2}$, with $\mathrm{Re}\left(k_{2q}^0\right) \geq 0$, R_q and T_q are the reflection and transmission coefficients of the qth Bloch wave, δ_q is Kronecker's delta, and L is the thickness of the acoustic metascreen.

The wave propagation in each slit is modeled by the TMM, in which the HRs are considered as 1D point scatterers [12,13]. Matrices describing the propagation in the slit, to the side-branch resonators, and to the section mismatch are assembled, giving the total transfer matrix [12,13]. The TMM assumes plane-wave propagation in each element, which is valid in the low-frequency regime. The radiation corrections are included in the impedances of the resonators to mimic the effect of the higher-order modes. Therefore, the wave propagation through the slit n can be modeled as

$$\begin{bmatrix} p^{(n)} \\ v_2^{(n)} \end{bmatrix}_{x_2=L} = \mathbf{T}^{(n)} \begin{bmatrix} p^{(n)} \\ v_2^{(n)} \end{bmatrix}_{x_2=0} = \begin{bmatrix} T_{11}^{(n)} & T_{12}^{(n)} \\ T_{21}^{(n)} & T_{22}^{(n)} \end{bmatrix} \begin{bmatrix} p^{(n)} \\ v_2^{(n)} \end{bmatrix}_{x_2=0}, \tag{5}$$

where $\mathbf{T}^{(n)}$ is given by the product of the transfer matrices of the N elements in the nth slit as

$$\mathbf{T}^{(n)} = \prod_{j=1}^{N} \mathbf{T}_j^{(n)}. \tag{6}$$

The transfer matrices, $\mathbf{T}_j^{(n)}$, are calculated according to the nature of the element (see the Supplemental Material [33]; see also Refs. [34–36]).

Once the acoustic fields inside each domain of the problem are defined, the continuity boundary conditions must be applied. These conditions read as follows:

$$p^{(0+)} = p^n \quad \text{on } \Gamma^n \text{ at } x_2 = L, \tag{7}$$

$$v_2^{(0+)} = v_2^n \quad \text{on } \Gamma^n \text{ at } x_2 = L, \tag{8}$$

$$v_2^{(0+)} = 0 \quad \text{on } \Gamma_s \text{ at } x_2 = L, \tag{9}$$

$$p^{(0-)} = p^n \quad \text{on } \Gamma^n \text{ at } x_2 = 0, \tag{10}$$

$$v_2^{(0-)} = v_2^n \quad \text{on } \Gamma^n \text{ at } x_2 = 0, \tag{11}$$

$$v_2^{(0-)} = 0 \quad \text{on } \Gamma_s \text{ at } x_2 = 0, \tag{12}$$

where Γ_s represents the rigid interfaces on the two faces of the metascreen and Γ^n is the interface between the nth slit

and the surrounding media $\Theta^{(0^+)}$ and $\Theta^{(0^-)}$. These conditions lead to a system of equations after projection on the adequate orthogonal modes. The system is solved for the scattering coefficients of the system (see the Supplemental Material [33]).

In order to validate this model, we employ a finite-element method (FEM) simulation using the COMSOL MULTIPHYSICS software to solve the scattering problem. A plane wave impinges the system and the complete geometry is considered using the radiation conditions that simulate the Sommerfeld conditions at the limits of the numerical domain.

In the model and in the FEM simulations, viscothermal losses are introduced via the effective parameters in every narrow region, i.e., the slits that compose the main waveguide and the resonators [37]. The effective bulk modulus and mass density of a slit of width h are given by

$$\rho_s = \rho_0 \left[1 - \frac{\tanh \frac{h}{2} G_\rho}{\frac{h}{2} G_\rho} \right]^{-1}, \tag{13}$$

$$\kappa_s = \kappa_0 \left[1 + (\gamma - 1) \frac{\tanh \frac{h}{2} G_\kappa}{\frac{h}{2} G_\rho} \right]^{-1}, \tag{14}$$

where h is the width of the slit, $G_\rho = \sqrt{i\omega\rho_0/\eta}$, $G_\kappa = \sqrt{i\omega \mathrm{Pr}\rho_0/\eta}$, γ is the specific heat ratio of the fluid, P_0 is the atmospheric pressure, Pr is the Prandtl number, η the dynamic viscosity, ρ_0 the fluid density, and $\kappa_0 = \gamma P_0$ the fluid bulk modulus, in our case air.

V. EXPERIMENTAL SETUP

The reflection and transmission coefficients of a symmetric scatterer can be recovered from four-microphone impedance-tube measurements as described in Ref. [38]. Figure 3(a) shows the square-cross-section impedance tube used for the characterization of the metascreen designed in this work. The cross section of the impedance tube has a surface of 150×150 mm^2, which allows the acoustic characterization of materials in the range of frequencies between 50 Hz and 1200 Hz. The impedance tube is terminated by an anechoic termination as shown in Fig. 3(a). The amplitude of the acoustic source is low enough to neglect the nonlinear behavior of the HRs.

VI. RESULTS

The model is used to calculate the absorption coefficient of the designed metascreen. This model is coupled with an optimization method [sequential quadratic programming (SQP) method] that varies the geometry of the system, providing structures with perfect absorption. The thickness of the metascreen, L, and the target frequency at which perfect absorption is desired are fixed in such a way that the system presents subwavelength dimensions. The geometric parameters for perfect absorption at 800 Hz with $\lambda/L \simeq 8$ are shown in Table I (where λ is the wavelength of the wave at the target frequency in air). Note that these fixed quantities impose $a_s = 2a_a = L$. Note also that the distance $d_0 = 148$ mm for the resonant building block is chosen to be slightly smaller than the side of the square impedance tube to allow a perfect fit of the sample using vacuum grease at the boundaries.

In this section, we explain, from a physical point of view, the steps in the optimization process to obtain perfect absorption in the transmission problem.

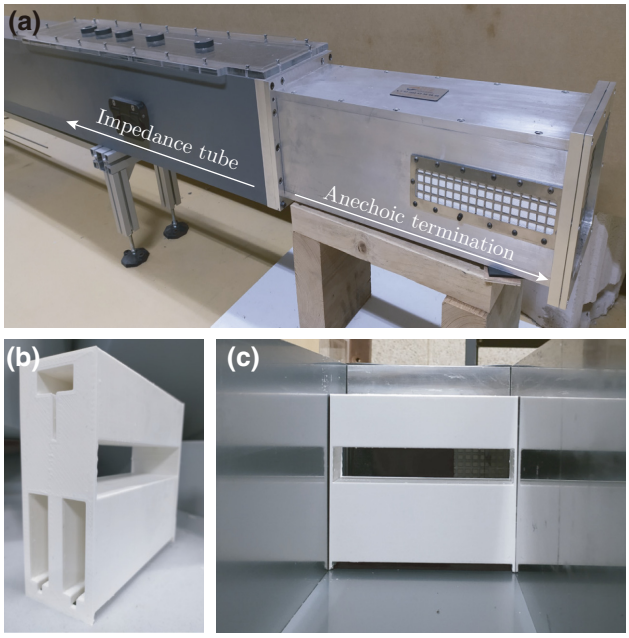

FIG. 3. (a) The impedance tube used for the acoustic measurements with the anechoic termination. (b) The 3D-printed symmetric resonant scatterer. (c) The symmetric resonant scatterer inside the impedance tube.

TABLE I. The geometric parameters for the symmetric and antisymmetric resonators of the metascreen for perfect absorption at 800 Hz.

a_s (mm)	h_s (mm)	w_{cs} (mm)	l_{cs} (mm)	w_{ns} (mm)	l_{ns} (mm)
53.6	29.8	25.45	12.9	2.4	25.1
a_a (mm)	h_a (mm)	w_{ca} (mm)	l_{ca} (mm)	w_{na} (mm)	l_{na} (mm)
26.8	6.6	16.05	58	4.2	7.1

A. Critical coupling of the symmetric and the antisymmetric problems

The antisymmetric slit supports two resonant modes, one symmetric and one antisymmetric, while the symmetric slit supports only one symmetric mode. Thus, due to the geometry considered in this work, only one antisymmetric resonant mode can be excited in the antisymmetric slit. Therefore, we start the discussion with the antisymmetric subproblem. Consider a Dirichlet condition in the mirror-symmetry plane of the metascreen. In the symmetric slit, only symmetric modes can be excited. Therefore, no modes will be excited inside this slit when imposing a Dirichlet boundary condition. However, in the antisymmetric slit, only the antisymmetric mode will be excited. Thus, the antisymmetric subproblem can be critically coupled by optimizing only the geometry of the antisymmetric slit. Figures 4(a) and 4(b) show the absolute value of the total acoustic field of the antisymmetric reflection problem at the frequency with perfect absorption. Only the antisymmetric slit is excited. The reflection and absorption coefficients of this problem are shown in Fig. 4(c). At the target frequency of 800 Hz, perfect absorption is obtained.

Once the antisymmetric subproblem is critically coupled, we have to consider the symmetric problem by imposing a Neumann boundary condition at the mirror-symmetry plane of the metascreen. In that case, symmetric modes exists in both slits. However, as the antisymmetric problem has been critically coupled by optimizing the geometry of the antisymmetric slit, now we only use the geometry of the symmetric slit to critically couple the symmetric subproblem. Figures 4(d) and 4(e) show the absolute value of the total acoustic field of the symmetric reflection problem at the frequency with perfect absorption. In this subproblem, the two resonators are excited. The reflection and absorption coefficients of this subproblem are shown in Fig. 4(f).

B. Perfect symmetric absorption

In the previous section, we critically couple the symmetric and the antisymmetric reflection subproblems. This means that the two eigenvalues of the scattering matrix vanish at the same frequency for the full transmission problem with the optimized geometry. Therefore, the full problem is critically coupled and perfect absorption is expected. The geometry obtained from the optimization problem for the complete resonator is used to 3D print the resonator as shown in Fig. 3(b). The resonator is mounted in the square-cross-section impedance tube [Fig. 3(c)] and

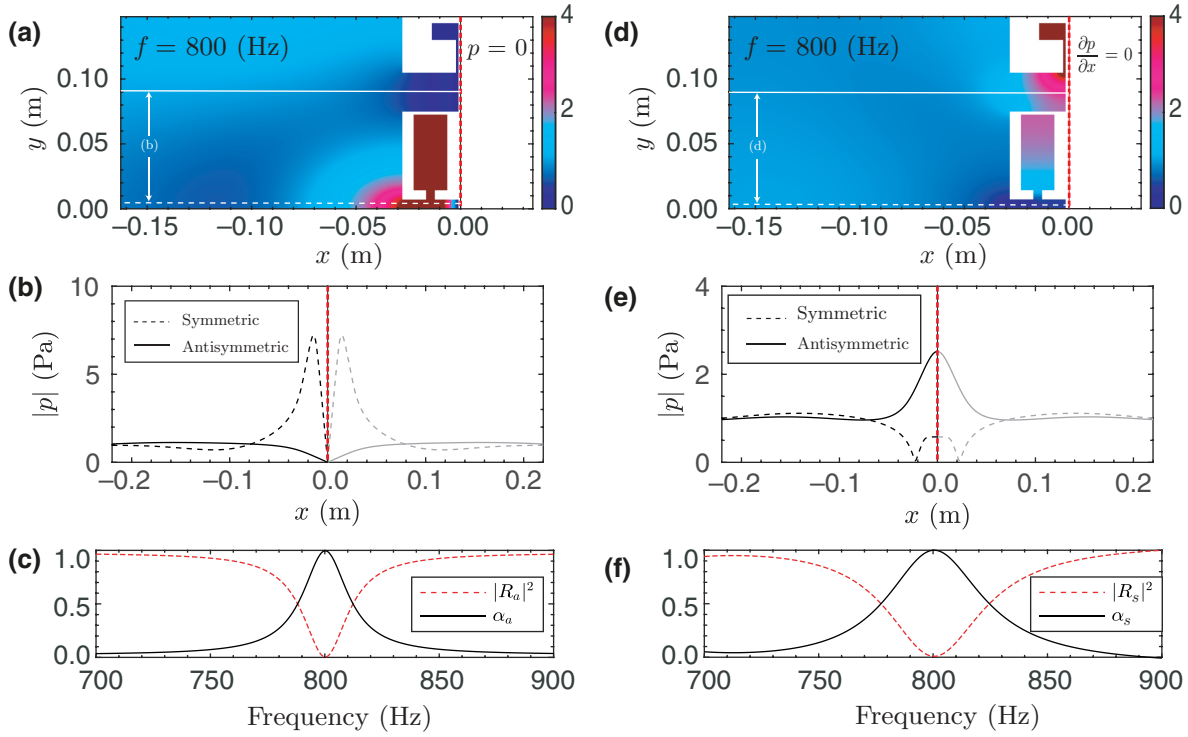

FIG. 4. The critical coupling of the symmetric and antisymmetric problem. (a) The absolute value of the total acoustic pressure field at perfect absorption of the antisymmetric problem. (b) The absolute value of the total pressure field, $|p|$, along the profiles shown in (a), considering the field in each slit for the antisymmetric problem. (c) The reflection and absorption coefficients of the antisymmetric problem. (d) The absolute value of the total acoustic pressure field at perfect absorption of the symmetric problem. (e) The absolute value of the total acoustic field, $|p|$, along the profiles shown in (c), considering the field in each slit for the symmetric problem. (f) The reflection and absorption coefficients of the symmetric problem.

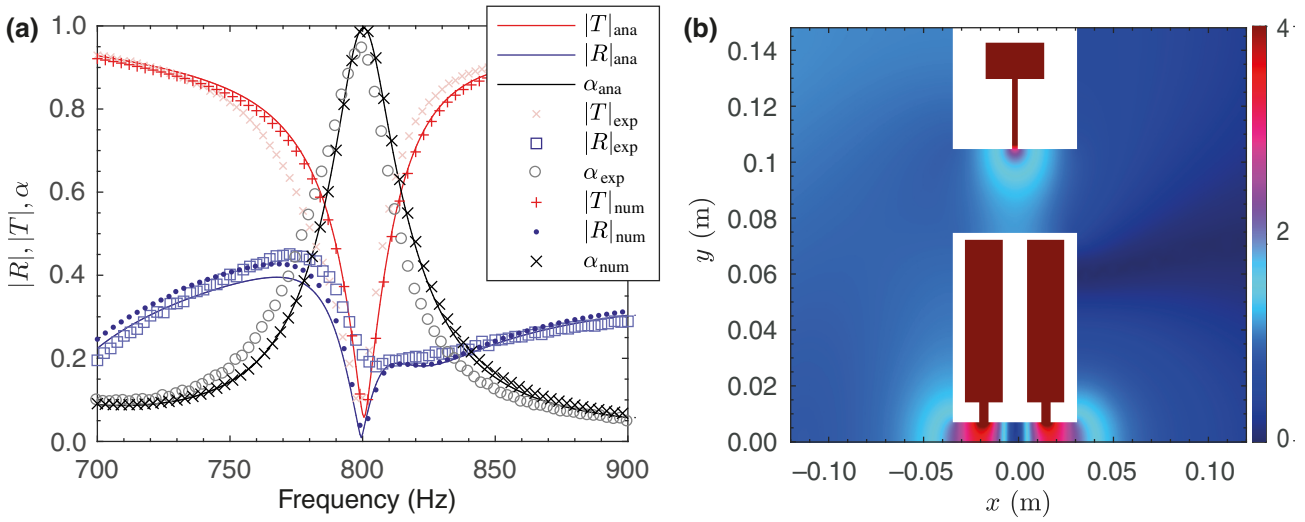

FIG. 5. (a) The analytical, numerical, and experimental scattering coefficients of the full problem. (b) The absolute value distribution of the acoustic field at perfect absorption of the full scattering problem.

the scattering parameters of the full problem are measured. It is worth noting here that the lateral walls of the structure are filled with Vaseline to avoid leakage through the lateral holes and to force the sound to pass by only via the slits.

Figure 5(a) shows the scattering coefficients of the full transmission problem. The agreement between the model, the numerical simulations, and the experimental results is very good. Note here that the presence of the Bloch waves is crucial in this kind of system: if only plane waves are accounted for in the system, the model does not reproduce the whole wave process because the evanescent coupling is neglected (see the Supplemental Material [33]). When the Bloch waves are considered, a perfect-absorption peak is observed at 800 Hz, as analytically, numerically, and experimentally observed. Figure 5(b) shows the acoustic field of the full problem at the perfect-absorption peak. It is worth noting here that perfect absorption is very sensitive to the geometry of the resonators and this would explain the slight discrepancies between the analytical or numerical predictions and the experimental results. The symmetric slit exhibits the symmetric Fabry-Pérot mode while the antisymmetric slit exhibits the antisymmetric Fabry-Pérot mode. Both modes are excited at the same frequency, i.e., the structure presents a degenerate resonance.

VII. CONCLUSIONS

Two subsystems with a degenerate resonance (symmetric for one and the other antisymmetric) are designed as the building blocks of an acoustic metascreen presenting perfect absorption independently of the incidence side. The resonant scattering produced by the metascreen is analytically studied by a hybrid model mixing the transfer-matrix and modal-decomposition methods and accounting for the Bloch waves in order to consider the possible coupling between the slits. Note that this coupling is particularly important for the present topology. If no higher-order Bloch waves are accounted for, i.e., if only the plane wave is accounted for outside the metascreen, the analytical model will not be in agreement with either the full-wave numerical simulation or the experimental results. The structure is experimentally tested in a square impedance tube, showing good agreement with the analytical and numerical predictions. Two facts should be highlighted. First, the metascreen is made of acoustically rigid materials, without any vibrating elements. The life duration of the present metascreen is thus expected to be longer than that of metascreens composed of membranes or plates. Second, the heights of the slits of the proposed metascreen are large enough for the system to be used in ventilation problems where air flow is of importance. The use of other types of resonators as 3D HRs will allow us to reach thinner structures with deeper subwavelength dimensions. The physics behind this work will motivate the development of broadband and perfect absorption for ventilation problems using cascade processes similar to the case of rainbow trapping for unidirectional absorption [13].

ACKNOWLEDGMENTS

We gratefully acknowledge the Agence Nationale de la Recherche (ANR)−Research Grants Council (RGC) METARoom project (Grant No. ANR-18-CE08-0021) and the HYPERMETA project, funded under the program Étoiles Montantes of the Région Pays de la Loire. This paper is based upon work from European Cooperation in Science and Technology (COST) Action DENORMS (Designs for Noise Reducing Materials and Structures) Grant No. CA15125, supported by COST. N.J. acknowledges financial support from the Spanish Ministry of

Science, Innovation, and Universities (MICINN) through the grant "Juan de la Cierva-Incorporación" (Grant No. IJC2018-037897-I).

[1] K. Y. Bliokh, Y. P. Bliokh, V. Freilikher, S. Savel'ev, and F. Nori, Colloquium: Unusual resonators: Plasmonics, metamaterials, and random media, Rev. Mod. Phys. **80**, 1201 (2008).

[2] T. S. Luk, S. Campione, I. Kim, S. Feng, Y. C. Jun, S. Liu, J. B. Wright, I. Brener, P. B. Catrysse, S. Fan, and M. B. Sinclair, Directional perfect absorption using deep subwavelength low-permittivity films, Phys. Rev. B **90**, 085411 (2014).

[3] J. R. Piper, V. Liu, and S. Fan, Total absorption by degenerate critical coupling, Appl. Phys. Lett. **104**, 251110 (2014).

[4] G. Ma, M. Yang, S. Xiao, Z. Yang, and P. Sheng, Acoustic metasurface with hybrid resonances, Nat. Mater. **13**, 873 (2014).

[5] P. Wei, C. Croënne, S. Tak Chu, and J. Li, Symmetrical and anti-symmetrical coherent perfect absorption for acoustic waves, Appl. Phys. Lett. **104**, 121902 (2014).

[6] J. Z. Song, P. Bai, Z. H. Hang, and Yun Lai, Acoustic coherent perfect absorbers, New J. Phys. **16**, 033026 (2014).

[7] V. Leroy, A. Strybulevych, M. Lanoy, F. Lemoult, A. Tourin, and J. H. Page, Superabsorption of acoustic waves with bubble metascreens, Phys. Rev. B **91**, 020301 (2015).

[8] Min Yang and Ping Sheng, Sound absorption structures: From porous media to acoustic metamaterials, Annu. Rev. Mater. Res. **47**, 83 (2017).

[9] V. Romero-García, G. Theocharis, O. Richoux, A. Merkel, V. Tournat, and V. Pagneux, Perfect and broadband acoustic absorption by critically coupled sub-wavelength resonators, Sci. Rep. **6**, 19519 (2016).

[10] V. Romero-García, G. Theocharis, O. Richoux, and V. Pagneux, Use of complex frequency plane to design broadband and sub-wavelength absorbers, J. Acoust. Soc. Am. **139**, 3395 (2016).

[11] Y. Li and B. M. Assouar, Acoustic metasurface-based perfect absorber with deep subwavelength thickness, Appl. Phys. Lett. **108**, 063502 (2016).

[12] N. Jiménez, W. Huang, V. Romero-García, V. Pagneux, and J.-P. Groby, Ultra-thin metamaterial for perfect and quasi-omnidirectional sound absorption, Appl. Phys. Lett. **109**, 121902 (2016).

[13] N. Jiménez, V. Romero-García, V. Pagneux, and J.-P. Groby, Rainbow-trapping absorbers: Broadband, perfect and asymmetric sound absorption by subwavelength panels for transmission problems, Sci. Rep. **7**, 13595 (2017).

[14] T. Lee, T. Nomura, E. M. Dede, and H. Iizuka, Ultrasparse Acoustic Absorbers Enabling Fluid Flow and Visible-Light Controls, Phys. Rev. Appl. **11**, 024022 (2019).

[15] Y. Aurégan, Ultra-thin low frequency perfect sound absorber with high ratio of active area, Appl. Phys. Lett. **113**, 201904 (2018).

[16] M. Yang, C. Meng, C. Fu, Y. Li, Z. Yang, and P. Sheng, Subwavelength total acoustic absorption with degenerate resonators, Appl. Phys. Lett. **107**, 104104 (2015).

[17] A. Merkel, G. Theocharis, O. Richoux, V. Romero-García, and V. Pagneux, Control of acoustic absorption in one-dimensional scattering by resonant scatterers, Appl. Phys. Lett. **107**, 244102 (2015).

[18] Junfei Li, Wenqi Wang, Yangbo Xie, Bogdan-Ioan Popa, and Steven A. Cummer, A sound absorbing metasurface with coupled resonators, Appl. Phys. Lett. **109**, 091908 (2016).

[19] Sibo Huang, Xinsheng Fang, Xu Wang, Badreddine Assouar, Qian Cheng, and Yong Li, Acoustic perfect absorbers via spiral metasurfaces with embedded apertures, Appl. Phys. Lett. **113**, 233501 (2018).

[20] Y. Duan, J. Luo, G. Wang, Z. H. Hang, B. Hou, J. Li, P. Sheng, and Y. Lai, Theoretical requirements for broadband perfect absorption of acoustic waves by ultra-thin elastic meta-films, Sci. Rep. **5**, 12139 (2015).

[21] X. Wang, X. Luo, H. Zhao, and Z. Huang, Acoustic perfect absorption and broadband insulation achieved by double-zero metamaterials, Appl. Phys. Lett. **112**, 021901 (2018).

[22] X. Ni, Y. Wu, Z.-G. Chen, L.-Y. Zheng, Y.-L. Xu, P. Nayar, X.-P. Liu, M.-H. Lu, and Y.-F. Chen, Acoustic rainbow trapping by coiling up space, Sci. Rep. **4**, 7038 (2014).

[23] C. Zhang and X. Hu, Three-Dimensional Single-Port Labyrinthine Acoustic Metamaterial: Perfect Absorption with Large Bandwidth and Tunability, Phys. Rev. Appl. **6**, 064025 (2016).

[24] M. Yang, S. Chen, C. Fu, and P. Sheng, Optimal sound-absorbing structures, Mater. Horiz. **4**, 673 (2017).

[25] M. Lanoy, R.-M. Guillermic, A. Strybulevych, and J. H. Page, Broadband coherent perfect absorption of acoustic waves with bubble metascreens, Appl. Phys. Lett. **113**, 171907 (2018).

[26] T. A. Starkey, J. D. Smith, A. P. Hibbins, J. R. Sambles, and H. J. Rance, Thin structured rigid body for acoustic absorption, Appl. Phys. Lett. **110**, 041902 (2017).

[27] J.-P. Groby, W. Huang, A. Lardeau, and Y. Aurégan, The use of slow waves to design simple sound absorbing materials, J. Appl. Phys. **117**, 124903 (2015).

[28] J.-P. Groby, R. Pommier, and Y. Aurégan, Use of slow sound to design perfect and broadband passive sound absorbing materials, J. Acoust. Soc. Am. **139**, 1660 (2016).

[29] R. Fleury, D. Sounas, and A. Alù, An invisible acoustic sensor based on parity-time symmetry, Nat. Commun. **6**, 5905 (2015).

[30] Y. Aurégan and V. Pagneux, $\mathcal{PT}$-Symmetric Scattering in Flow Duct Acoustics, Phys. Rev. Lett. **118**, 174301 (2017).

[31] N. Jiménez, V. Romero-García, V. Pagneux, and J.-P. Groby, Quasiperfect absorption by subwavelength acoustic panels in transmission using accumulation of resonances due to slow sound, Phys. Rev. B **95**, 014205 (2017).

[32] L. Chesnel and V. Pagneux, Simple examples of perfectly invisible and trapped modes in waveguides, Q. J. Mech. Appl. Math. **71**, 297 (2018).

[33] See the Supplemental Material at http://link.aps.org/supplemental/10.1103/PhysRevApplied.14.054055 for the modal decomposition used to analyze the propagation through the acoustic metasurface.

[34] Vincent Dubos, J. Kergomard, A. Khettabi, J.-P. Dalmont, D. H. Keefe, and C. J. Nederveen, Theory of sound

propagation in a duct with a branched tube using modal decomposition, Acta. Acust. United Acust. **85**, 153 (1999).

[35] J. Kergomard and A. Garcia, Simple discontinuities in acoustic waveguides at low frequencies: Critical analysis and formulae, J. Sound Vib. **114**, 465 (1987).

[36] G. Theocharis, O. Richoux, V. Romero-Garcìa, A. Merkel, and V. Tournat, Limits of slow sound and transparency in lossy locally resonant periodic structures, New J. Phys. **16**, 093017 (2014).

[37] M. R. Stinson, The propagation of plane sound waves in narrow and wide circular tubes, and generalization to uniform tubes of arbitrary cross-sectional shape, J. Acoust. Soc. Am. **89**, 550 (1991).

[38] M. Niskanen, J.-P. Groby, A. Duclos, O. Dazel, J. C. Le Roux, N. Poulain, T. Huttunen, and T. Lähivaara, Deterministic and statistical characterization of rigid frame porous materials from impedance tube measurements, J. Acoust. Soc. Am. **142**, 2407 (2017).